# Nanoscale surface charge detection in epoxy resin materials using electrostatic force spectroscopy

D. El Khoury, R. Arinero, J. Laurentie, J. Castellon

# Nanoscale surface charge detection in epoxy resin materials using electrostatic force spectroscopy

Cite as: AIP Advances **6**, 035318 (2016); https://doi.org/10.1063/1.4944953
Submitted: 24 September 2015 . Accepted: 16 March 2016 . Published Online: 24 March 2016

D. El Khoury, R. Arinero, J. C. Laurentie, and J. Castellon

# Nanoscale surface charge detection in epoxy resin materials using electrostatic force spectroscopy

D. El Khoury, R. Arinero,[a] J. C. Laurentie, and J. Castellon
*Institut d'Electronique et des Systèmes (IES), UMR CNRS 5214, Université de Montpellier, CC 05-004, Campus Saint Priest, 34095 Montpellier Cedex, France*

(Received 24 September 2015; accepted 16 March 2016; published online 24 March 2016)

Electrostatic force spectroscopy (EFS) operated in a conventional force gradient detection method allows determining local surface charges in epoxy samples. This is made possible through a detailed analysis of gradient versus DC voltage curves. The parabolic dependence of these curves is closely related to the charge density. Both maximum and origin-ordinate are key data from which it is possible to extract quantitative information on the detected charge. The study is based on the combined use of numerical and analytical simulations of the probe sample interaction. Excellent sensitivities to very low surface charge densities are reported. 
[http://dx.doi.org/10.1063/1.4944953]

## I. INTRODUCTION

While a biased atomic force microscopy probe is scanned over a sample surface, it is possible to generate an image contrast related to nanoscale electric or dielectric surface properties. Such techniques are known under the name of electrostatic force microscopy (EFM). If the probe is maintained in a fixed position, electrostatic force spectroscopy (EFS) consists of measuring and quantifying such properties at or around this point.

EFM is a well-established technique[1,2] which has already proved to be successful in various application areas. EFM is, for example, routinely used to determine surface potentials of doped semiconductors[3]; such measurements are now possible under vacuum thanks to the excitation of higher order harmonics, that allow reducing the stabilization time (transient regime) of the oscillating sensor.[4] EFM is also widely used in the form of the Kelvin Probe Force Microscopy (KPFM) variant[5] which can be sensitive to the composition and electronic state of the local structure up to atomic or molecular scales.[6,7] An important advance in EFM technique was achieved by Crider et al.[8,9] and Riedel et al.[10] who developed the so-called local dielectric spectroscopy (LDS), based on the detection of the phase shifts of AC gradients under vacuum which allowed studying dielectric losses in thin polymer layers. This approach was recently extended to ambient conditions, under the name of nanoDielectric Spectroscopy (nDS) by Schwartz et al.,[11] by detecting AC forces over 4 decades. We can also mention substantial progress made toward studying nanowires and nanotubes properties.[12]

In addition, EFS is becoming a tool of primary importance in electrical engineering for the study of charge injection and retention in dielectrics. Although the electric field penetrates into the sample, EFS measurements remain concentrated at the surface; thus, the detected charge can be considered as a surface charge. We can mention the work of Villeneuve-Faure et al[13] who have studied the profile width of KPFM signals related to the dissemination of injected charges depending on the ratio between the gas flow rates used during the synthesis of silicon oxynitride ($SiO_xN_y$) layers.

The same authors have recently proposed another technique: the electrostatic force distance curve (EFDC)[14] which is based on the analysis of standard force distance curves while the AFM probe is biased with a DC voltage. Such method has demonstrated an excellent sensitivity for the detection of surface charges but has only been proposed for spectroscopy and not yet for imaging. In

[a]Corresponding author: Richard.Arinero@umontpellier.fr

 

this paper we rely on the fact that conventional gradient-based methods (Amplitude-Modulation[15] or Frequency-Modulation[10]), which are recognized for their ability to imaging dielectric properties, are also well adapted to perform high-sensitivity EFS of surface charge by means of electrostatic force gradient versus DC voltage curves, i.e. by using phase or frequency detuning, respectively. Such curves have, for example, been used for the study of charge trapping in MOS structures[16] or in carbon nanotubes,[17] and to determine the charge state of an adatom.[18] It is worth to mention that the maximum in the parabolic dependence of gradient versus DC voltage curves can be directly obtained in KPFM provided it is located in the measurement interval. A sophisticated numerical model was proposed by Gomez *et al* [19] to estimate the surface charge density and the dielectric constant of hemispherical samples from force gradient measurements.

We describe experiments conducted on very common materials in electrical engineering: epoxy resins. Measuring space charge densities in this kind of material dedicated to electrical insulation is crucial. In fact, space charges generate an additional electric field which locally disturbs the applied field, and may lead, across the insulation, to field distributions significantly different from the ones calculated in the absence of space charge. The effect of space charge accumulation in an insulating material can be highly detrimental, going from premature ageing to dielectric breakdown. The real distribution of the electric field (applied field added to the field due to space charge) is therefore a parameter to be taken into account for an optimal design and operation of the insulation.[20] In recent years, several non-destructive techniques for measuring space charge in solid insulations have been set up[21,22] with a micrometric resolution in the best case. Improving the resolution toward the nanometric scale is still a challenge that could find an answer with EFS. Contrarily to the previously mentioned methods, we show in this paper that it is possible to detect a surface charge without preliminary injection.

## II. EXPERIMENTAL AND THEORETICAL BACKGROUNDS

When the EFS probe is biased with respect to a grounded conductive substrate, an electric field is produced at the vicinity of the surface. The field lines are concentrated around the tip apex[23] in such a way that one can consider that an electrostatically coupled circular area of radius $R_c$ is created as represented in Figure 1(a).

EFS signals are manifested by a parabolic dependence of mechanical phase and frequency shifts in response to a DC voltage difference between the probe and the conductive substrate.[4,24] The parabola aperture coefficient can be used to determine the local dielectric permittivity in the case of thin dielectric film sample[24] whereas the voltage value at the maximum of the parabola has already been associated with the trapped charge density in irradiated oxides.[25]

In our experiments, the samples consisted of pure epoxy films of thickness h = 2 mm. The epoxy resin was diglycidyl ether of bisphenol A (DGEBA) based resin, commercially known as DER332. The selected hardener was poly (propylene glycol) bis (2-aminopropyl ether) (PPG-b-AP) and (3-Glycidyloxypropyl) triethoxysilane (GOPTES) was used as a coupling agent. The chosen

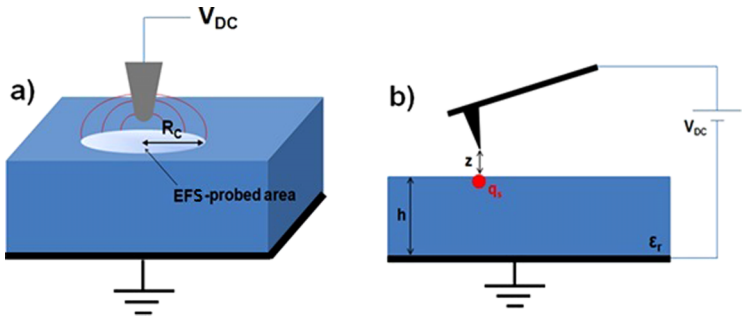


FIG. 1. a) Schematic representation of the electrostatically coupled area by the EFS probe under DC bias polarization at a fixed distance value, b) Equivalent charge associated with the coupled area.

organoclay was Cloisite 30B (a natural montmorillonite (MMT) modified with a quaternary ammonium ion (MT2etOH - methyl, tallow, bis-2- hydroxyethyl, quaternary ammonium)). The surface topography was related with the extrusion process and the typical root mean square roughness measured from AFM 1 μm scans was less than 10 nm. The film was just affixed to a metallic disk and no specific treatment was done on the surface. A typical value of the dielectric permittivity for an epoxy resin is $\varepsilon_r = 3.6$.[26]

EFS was performed with a commercial AFM (Bruker, previously Veeco, Enviroscope™) in air atmosphere at room temperature using the so-called " double-pass method ".[4] The electrostatic force gradient $Grad\, F_{DC}$ was detected during the second scan, while a potential $V_{DC}$ was applied to the tip (with the sample holder grounded (Figure 1)). The force gradient was obtained directly from the measurement of the resonance frequency shift $\Delta f_0$ keeping the phase shift constant,[4] using relation:

$$\frac{\Delta f_0}{f_0} \cong -\frac{1}{2}\frac{Grad\, F_{DC}}{k_c} \quad , \tag{1}$$

where $k_c$ is the stiffness of the cantilever.

In a first approximation we consider that the probe-sample arrangement is axisymmetric (Figure 1(a)), it is then intuitive to assimilate the surface charges detected by the AFM probe to an equivalent punctual charge $q_s$, as represented in Figure 1(b). As explained further (section III), the value of $q_s$ is related to the EFS coupled area (*i.e.* ultimately to the probe geometry and the probe to surface distance). The image charge on the probe is given by $q_t = -q_s + q_{DC}$ , where $q_{DC} = CV_{DC}$ corresponds to the induced capacitive charge.

The force acting on the probe can be expressed as[27]:

$$F_{DC} = \frac{1}{2}C'V_{DC}^2 + \frac{q_s q_t}{4\pi\varepsilon_0 z^2} \tag{2}$$

*i.e.* as the sum of a capacitive and a Coulombian contribution.

We considered that the value of the contact potential (work function difference between the probe and the substrate) which is only about few tens of mV can be neglected in equation (2). Indeed, as it will be shown later in the experimental section, it has very small influence on the parabolic response in our present case.

By differentiating expression (2) we obtain:

$$Grad\, F_{DC} = \frac{1}{2}C''V_{DC}^2 + \frac{q_s}{4\pi\varepsilon_0}\left(\frac{C'}{z^2} - \frac{2C}{z^3}\right)V_{DC} + \frac{q_s^2}{2\pi\varepsilon_0 z^3} \tag{3}$$

where $C = C(z+h)$, $C' = \frac{\partial C(z+h)}{\partial z}$ and $C'' = \frac{\partial^2 C(z+h)}{\partial z^2}$ are respectively the probe to substrate capacitance, the first and the second derivative.

Thus, the resonance frequency shift can be expressed by a second order polynomial function of $V_{DC}$ (whose coefficients are α, β and γ), such as:

$$\Delta f_0 = -\frac{f_0}{2k_c}Grad\, F_{DC} = \alpha V_{DC}^2 + \beta V_{DC} + \gamma = \alpha\left(V_{DC} + \frac{\beta}{2\alpha}\right)^2 + \gamma - \frac{\beta^2}{4\alpha} \tag{4}$$

where $\gamma = \Delta f_0(V_{DC} = 0)$. As represented in Figure 2(a), a parabolic profile of $\Delta f_0(V_{DC})$ curves is expected with a maximum $P_{max}$ at a voltage value around $-\frac{\beta}{2\alpha}$. The absolute value of the equivalent charge $q_s$ can be deduced from the knowledge of γ by combining equations (3) and (4):

$$|q_s| = \sqrt{\frac{|\gamma|}{f_0}4\pi\varepsilon_0 k_c z^3} \tag{5}$$

## III. EXPERIMENTAL RESULTS AND NUMERICAL SIMULATIONS

An example of experimental curve obtained on a 2 mm thick epoxy sample at a tip to sample distance z = 215 nm is shown in Figure 2(b). The parameters of the probe used for this experiment

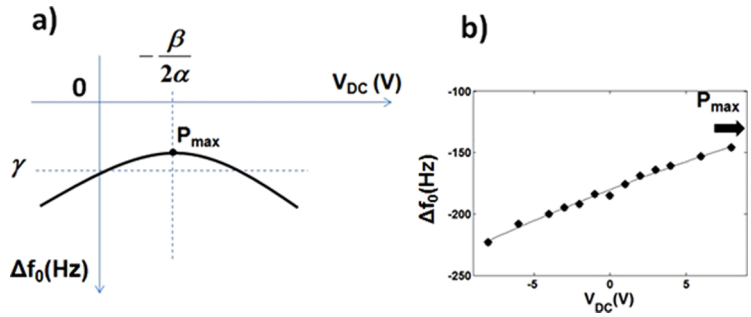


FIG. 2. (a) Theoretical parabolic profile of $\Delta f_0(V_{DC})$ curve. b) Example of experimental $\Delta f_0(V_{DC})$ curve recorded on a 2 mm thick epoxy resin sample at a tip to sample distance z = 215 nm.

are $k_c \approx 3$ N.m$^{-1}$ and $f_0 \approx 70$ kHz. It is composed of 30 nm thick PtIr coating on both reflector and tip tide, and the tip radius is about 50 nm. For an applied voltage ranging from -8V to +8V, we only observe a single branch of the parabola and one notices that the maximum is not reached. This indicates that the space charge is significant enough to shift the maximum outside the measurement interval.

Numerical simulations were carried out using the 2D axisymmetric solver available in the AC/DC module of COMSOL Multiphysics® software. They are illustrated in Figure 3 where an example of calculated force-distance F(z) curve and equipotential lines is shown, when the probe is biased at 1V and R = 50 nm. As described in Ref. 28, simulation area of circular shape was considered with a large diameter compared to the dimensions of the probe-sample arrangement. A zero charge boundary condition was selected for this area and also at symmetry boundaries where the potential is known to be symmetric with respect to the boundary. A constant potential was assumed on the probe surface, whereas the metallic substrate was grounded. In the simulations, we modelled the cantilever as a simple disc (Inset of Figure 3), although in fact it has rectangular or triangular shape. This simplification gives a good approximation, provided that the disc radius is chosen properly (typically a disk of 30 μm diameter).[29]

These simulations allowed calculating F(z) curves from which it was possible to deduce the values of C, C' and C". The sign of the surface charge was then determined from the expression of the abscissa at the maximum of the parabola after combining equations (3) and (4). From

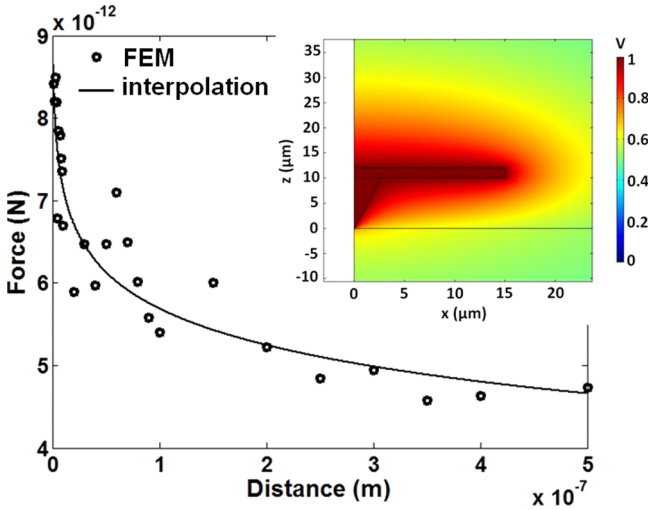


FIG. 3. Electrostatic force versus distance curve calculated by finite element method (COMSOL Multiphysics® software) with $V_{DC}$ = 1V and R = 50 nm. Inset: probe-sample arrangement and equipotential lines.

equation (3), it comes by identification that α and β in equation (4) can be expressed respectively as:

$$\alpha = -\frac{f_0}{4k_c}C'' \text{ and } \beta = -\frac{f_0}{2k_c}\frac{q_s}{4\pi\varepsilon_0}\left(\frac{C'}{z^2} - \frac{2C}{z^3}\right)$$

Thus, we can deduce that:

$$-\frac{\beta}{2\alpha} = \frac{q_s}{4\pi\varepsilon_0}\frac{1}{C''}\left(\frac{2C}{z^3} - \frac{C'}{z^2}\right) \tag{6}$$

where $\frac{1}{C''}\left(\frac{2C}{z^3} - \frac{C'}{z^2}\right)$ is always found to be positive. Thus, we deduce that $q_s > 0$ when $-\frac{\beta}{2\alpha} > 0$ and *vice versa*. Accordingly, the surface charge measured in Figure 2(b) is positive.

In Figure 4, experimental $\Delta f_0(V_{DC})$ curves obtained on epoxy samples at different tip to sample distances are reported. Two different trends can be observed depending on the position of the probe over the sample. An example of the first trend is given in Figure 4(a): when increasing the tip to sample distance, we observe that the branch of parabola always shows a positive slope and is offset toward lower values of frequency shifts. At the same time, the shape of the curve suggests that $P_{max}$ is shifted toward higher positive voltage values. Both effects can be interpreted as an increasing equivalent charge. This phenomenon is explained, assuming a constant surface charge density, by the fact that the electrostatically coupled area of radius $R_c$, illustrated in Figure 1(a), increases with the distance according to the following relation[23]:

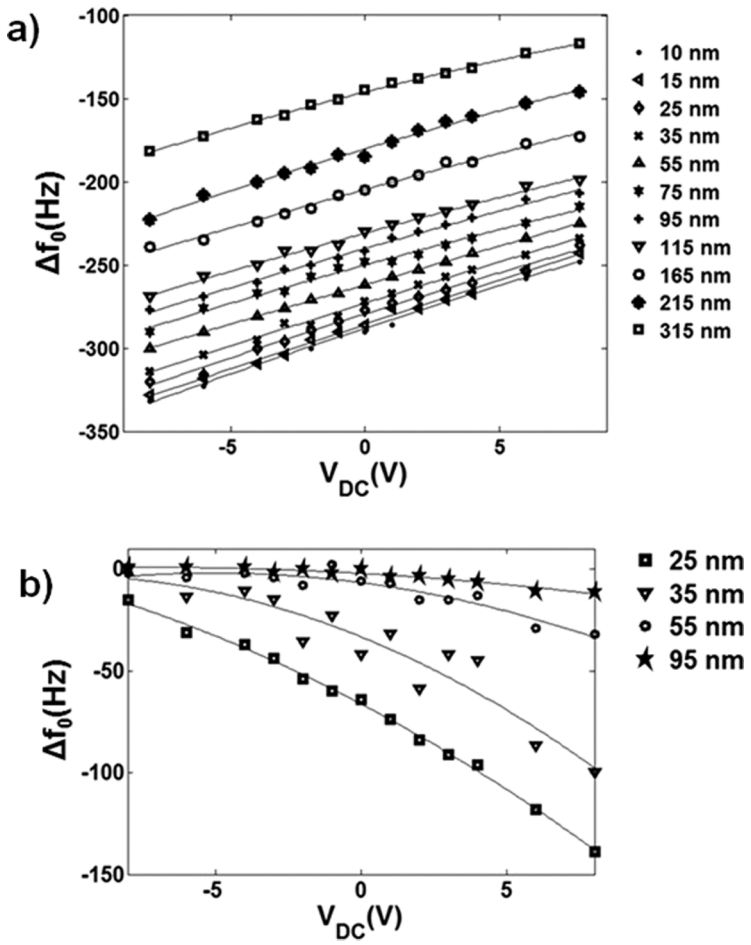


FIG. 4. (a) Experimental $\Delta f_0(V_{DC})$ curves obtained on epoxy samples at different tip to sample distances with a positive charge density. (b) Same curves obtained with a negative charge density. The lines are guides for the eyes.

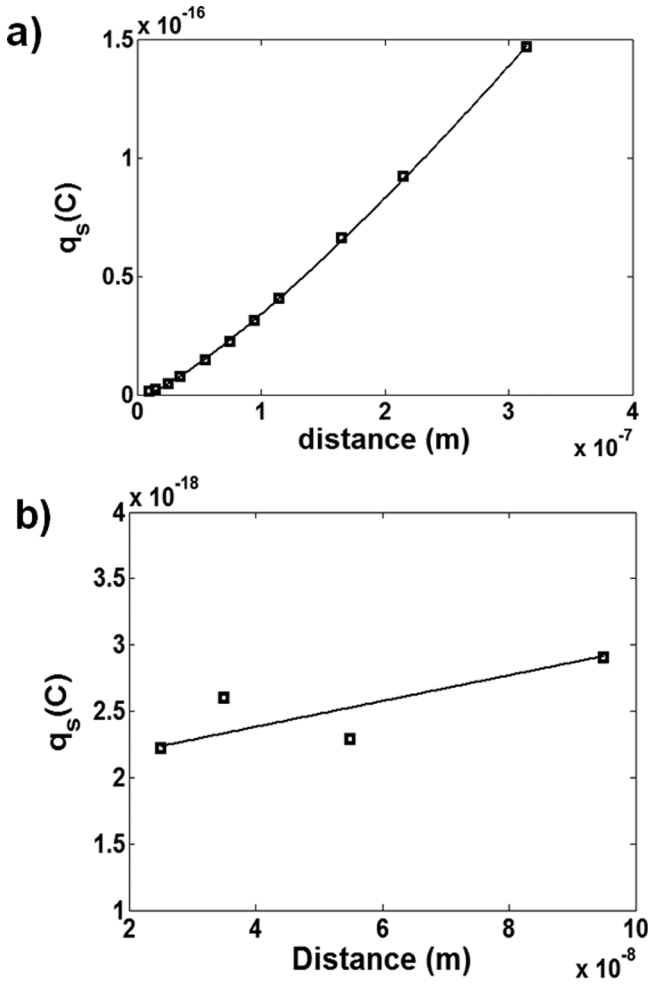


FIG. 5. (a) Equivalent punctual charge values $q_s$ calculated (relation (5)) from the ordinate-origin intersection of $\Delta f_0(V_{DC})$ curves in the case of positive slope (Figure 4(a)). (b) Same kind of calculation in the case of negative slope (Figure 4(b)).

$$R_c = R\left[cos\theta + \left(1 - sin\theta + \frac{z}{R}\right)\left(\frac{1}{cos\theta} - tan\theta\right)\right] \tag{7}$$

where θ is the half-cone angle of the probe tip. Typically, $R_c$ varies from 100 to 350 nm when z increases from 20 to 300 nm. Consequently, if $q_s$ increases with the distance, then, using equations (3) and (4), it is possible to explain the general offset of frequency shifts and $P_{max}$ values, from theoretical expressions of γ and $-\frac{\beta}{2\alpha}$ respectively.

Equivalent punctual charge values $q_s$ were extracted from the ordinate-abscissa intersection γ of plots in Figure 4 according to relation (5). We observed two trends depending on whether $q_s > 0$ (Figure 4(a)) or $q_s < 0$ (Figure 4(b)). The corresponding absolute values of $q_s$ are reported in Figure 5(a) and 5(b), respectively. In Figure 5(a), an important charge increase from $1e^{-18}$ to $1.5e^{-16}$ C is observed for z = 10 to 315 nm. Using relation (7), we can estimate that during the experiment the probe was sensitive to an average value of surface charge density $\sigma_s = q_s/\pi R_c^2 = 2.5e^{-4}$ C/m$^2$.

In Figure 4(b), we can observe that the branch of parabola has a negative slope and so that $P_{max}$ tends to a negative voltage becoming higher at progressively increasing distance. Corresponding $q_s$ values, given in Figure 5(b), are significantly less than those obtained in Figure 5(a). For distances ranging from 25 to 95 nm, $q_s$ slightly varies from $2.2e^{-18}$ to $2.8e^{-18}$ C. We note that the measured values are very low and that, consequently, it becomes impossible to detect a frequency shift beyond z = 95 nm. In terms of surface charge density, this one is evaluated to approximately $\sigma_s = -5e^{-5}$ C/m$^2$, *i.e.* much smaller compared to positive densities.

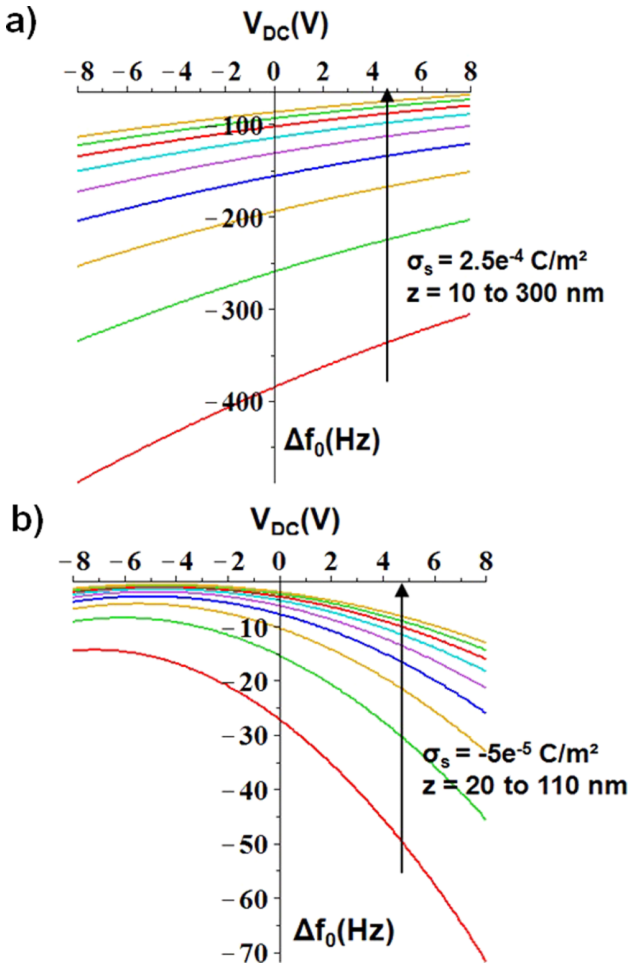


FIG. 6. (a) Theoretical prediction of $\Delta f_0(V_{DC})$ curves at different tip to sample distances for a particular positive value of the surface charge density. (b) Same simulation performed at a smaller negative charge density.

The numerical simulations previously mentioned (calculation of C, C'and C") associated with analytical modelling (calculation of $R_c$) allowed accounting for the performed experiments. Indeed, as reported on Figure 6(a), it was possible to show that origin-ordinate voltages and $P_{max}$ positions for high positive surface charge densities ($\sigma_s$ = 2.5e$^{-4}$ C/m$^2$) and z increasing from 10 to 300 nm, $\Delta f_0(V_{DC})$ curves are accurately predicted in the range of -400 Hz to -100 Hz. The same corroboration was done regarding low negative charge densities ($\sigma_s$ = -5e$^{-5}$ C/m$^2$) measurements, as reported on figure 6(b).

## IV. CONCLUSION

In conclusion, we have studied the parabolic dependence of electrostatic force gradients to DC bias voltages on epoxy layers without preliminary charge injection. These curves showed an excellent sensitivity to the surface charge, even at very low charge densities. We could show a trend that emerges depending on the sign of the charge and we were able to provide an order of magnitude of its value. This was made possible through detailed analysis of the curves associated with numerical and analytical modelling of the probe surface capacitance and the electrostatically coupled area, respectively.

This method will offer opportunities for studying insulations used in electrical engineering and especially for new types of materials such as micro[30] and nanocomposites[31] for which it should be particularly suited for localization (imaging) of charges around the particles.

## ACKNOWLEDGEMENTS

This work was supported by the French ministry of education and research and the doctoral school "information, structures and systems" (I2S) of the university of Montpellier, France (grant to D. EK). We would like to acknowledge the technical support provided by Dr Michel Ramonda in the frame of the "centre de technology" (CTM) of the University of Montpellier, France.

[1] Y. Martin and H. K. Wickramasinghe, Appl. Phys. Lett. **50**, 1455 (1987).
[2] M. Nonnenmacher, M.P. Oboyle, and H.K. Wickramasinghe, Appl. Phys. Lett. **58**, 2921 (1991).
[3] H. O. Jacobs, H. F. Knapp, S. Muller, and A. Stemmer, Ultramicroscopy **69**(1), 39–49 (1997).
[4] L. Portes, P. Girard, R. Arinero, and M. Ramonda, Review of Scientific Instruments **77**, 096101 (2006).
[5] P. Girard, Nanotechnology **12**, 485-490 (2001).
[6] W. Melitz, J. Shen, A. C. Kummel, and S. Lee, Surf. Sci. Rep. **66**, 1-27 (2011).
[7] C. Barth, A. S. Foster, C. R. Henry, and A. L. Shluger, Adv. Mater. **23**, 477-501 (2011).
[8] P. S. Crider, M. R. Majewski, J. Zhang, H. Oukris, and N. E. Israeloff, Appl. Phys. Lett. **91**, 013102 (2007).
[9] P. S. Crider, M. R. Majewski, J. Zhang, H. Oukris, and N. E. Israeloff, J. Chem. Phys. **128**, 044908 (2008).
[10] C. Riedel, R. Sweeney, N. E. Israeloff, R. Arinero, G. A. Schwartz, A. Alegria, P. Tordjeman, and J. Colmenero, Appl. Phys. Lett. **96**, 213110 (2010).
[11] G. A. Schwartz, C. Riedel, R. Arinero, Ph. Tordjeman, A. Alegria, and J. Colmenero, Ultramicroscopy **111**(8), 1366–1369 (2011).
[12] T. Melin, M. Zdrojek, and D. Brunel, "Electrostatic Force Microscopy and Kelvin Force Microscopy as a Probe of the Electrostatic and Electronic Properties of Carbon Nanotubes," *Scanning Probe Microscopy in Nanoscience and Nanotechnology* (Springer-Verlag Berlin Heidelberg, 2010), pp. 89-128.
[13] C. Villeneuve-Faure, K. Makasheva, C. Bonafos, B. Despax, L. Boudou, P. Pons, and G. Teyssedre, J. Appl. Phys. **113**, 204102 (2013).
[14] C. Villeneuve-Faure, L. Boudou, K. Makasheva, and G. Teyssedre, J. Phys. D: Appl. Phys. **47**, 455302 (2014).
[15] C. Riedel, R. Arinero, P. Tordjeman, G. Lévêque, G. A. Schwartz, A. Alegría, and J. Colmenero, Phys. Rev. E **81**, 010801R (2010).
[16] R. Dianoux, F. Martins, F. Marchi, C. Alandi, F. Comin, and J. Chevrier, Phys. Rev. B **68**, 45403 (2003).
[17] M. Paillet, P. Poncharal, and A. Zahab, Phys. Rev. Lett. **94**, 186801 (2005).
[18] L. Gross, F. Mohn, P. Liljeroth, J. Repp, F. J. Giessibl, and G. Meyer, Science **324**, 1428 (2009).
[19] A. Gomez, A. Avila, and J. P. Hinestroza, J. Electrostat. **68**, 79-84 (2010).
[20] P. Notingher, A. Toureille, S. Agnel, and J. Castellon, IEEE Transactions on Industry Applications **45**(1), 67 (2009).
[21] G. M. Sessler, IEEE Trans. IEEE Transactions on Dielectrics and Electrical Insulation **4**(5), 614 (1997).
[22] N. H. Ahmed and N. N. Srinivas, IEEE Transactions on Dielectrics and Electrical Insulation **4**(5), (1997).
[23] P. Girard and A. N. Titkov, in *Applied scanning probe methods II*, edited by B. Bhushan and H. Fuchs (Springer, 2003), p. 312.
[24] C. Riedel, R. Arinero, P. Tordjeman, M. Ramonda, G. Lévêque, G. A. Schwartz, D. G. de Oteya, A. Alegría, and J. Colmenero, J. Appl. Phys. **106**, 024315 (2009).
[25] H. Dongmo, J.F. Carlotti, G. Bruguier, C. Guasch, J. Bonnet, and J. Gasiot, Applied Surface Science **212–213**, 607–613 (2003).
[26] Resources, Tools and Basic Information for Engineering and Design of Technical Applications: http://www.engineeringtoolbox.com/.
[27] D. Sarid, in *Scanning Force Microscopy with Applications to Electric, Magnetic and Atomic Forces*, edited by M. Lapp and H. Stark (Oxford University Press, New York, 1991).
[28] R. Arinero, C. Riedel, and C. Guasch, J. Appl. Phys. **112**, 114313 (2012).
[29] G Gramse, G Gomila, and L Fumagalli, Nanotechnology **23**, 205703 (2012).
[30] A. Krivda, T. Tanaka, M. Frechette, J. Castellon, D. Fabiani, G.C. Montanari, R. Gorur, P. Morshuis, S. Gubanski, J. Kindersberger, A. Vaughn, S. Pelissou, Y. Tanaka, L.E. Schmidt, G. Iyer, T. Andritsch, J. Seiler, and M. Anglhuber, IEEE Electrical Insulation Magazine **28**(2), 38 (2012).
[31] I. Preda, J. Castellon, S. Agnel, H. Couderc, M. Fréchette, F. Gao, R. Nigmatullin, S. Thompson, and A. F. Vaessen, IEEE Transactions on Dielectrics and Electrical Insulation **20**(2), 580 (2013).